

High-Temperature Workability of Thixocast A356 Aluminum Alloy



SHAILESH KUMAR SINGH, K. CHATTOPADHYAY, and PRADIP DUTTA

The present work highlights the role of globular microstructure on the workability of A356 aluminum alloy at elevated temperature. The hot deformation behavior was studied by isothermal hot compression tests in the temperature range 573 K to 773 K (300 °C to 500 °C) and strain rate range of 0.001 to 10 s⁻¹. The flow stress data obtained from the tests were used to estimate the strain rate sensitivity and strain rate hardening. Flow stress analysis of the alloy shows that the effect of temperature on strain hardening is more significant at lower strain levels and strain rate sensitivity is independent of strain. The results also reveal that the flowability of conventionally cast alloy increases after changing the dendritic microstructure into a globular structure through semisolid processing route. Thixocast alloy exhibits lower yield strength and higher elongation at elevated temperature in comparisons to conventionally cast values. This property has an important implication toward thixo-forming at an elevated temperature.

DOI: 10.1007/s11661-015-2855-y

© The Minerals, Metals & Materials Society and ASM International 2015

I. INTRODUCTION

ALUMINUM-SILICON alloys are known for their good castability and corrosion resistance properties. In this alloy series, A356 (Al-7pctSi-0.3pctMg) has excellent properties for cast aluminum and is used to produce several critical parts which require high strength, elongation, and light weightness.^[1] Generally, the processing techniques for these types of alloys are either carried out in liquid state (such as in sand casting and die casting) or in solid state (such as in forging and extrusion). In liquid state processing, solidification is dendritic in nature which results in deterioration of mechanical properties of the cast products. On the contrary, the forged products are superior in terms of mechanical properties, but their applications are limited because of the requirement of high press capacity, short die life, and forming limitations. To overcome the above drawbacks, semisolid manufacturing, which can produce parts of the almost near desired shape and with superior mechanical properties, has been studied widely as a possible alternative. These processes are often known in the literature as Rheocasting or Thixocasting, depending on the semisolid processing route.^[2–8] Thixocasting is basically a two step process, which involves preparation of non-dendritic feedstock material and then reheating the feedstock material to semisolid temperature. Subsequently, the reheated feedstock is injected into a closed die, as in high pressure die casting,

to obtain the required shaped components. Rheocasting, on the other hand, involves preparation of semisolid slurry from liquid alloys by shearing during solidification and transferring the semisolid slurry directly into a die or mold for component shaping.

Mechanical processing is a significant step required for shaping a material into engineering components with better surface finish and superior mechanical properties. Generally, these mechanical processing techniques such as rolling, forging, forming, and extrusion are carried out at high temperature so that large deformation can be provided without commencement of fracture. The engineering parameter of importance which determines the ease with which metal can be shaped through the plastic deformation process is termed as workability. Hence, understanding of workability is important to address the degree of deformation that can be attained in a particular metalworking process without any cracking, fracture, or degradation of mechanical properties. Generally, workability is dependent on strain, strain rate, temperature, and flow characteristics of the material. Consequently, it is appropriate to classify hot workability as *intrinsic* workability which depends on the previous history of the material, temperature, strain and strain rate of working, and *state-of-stress* workability which depends primarily on die design. A suitable combination of these two types of workability is required to produce a product with desirable mechanical properties. For materials with poor intrinsic workability, optimization of both intrinsic workability and state-of-stress workability is essential. While the state-of-stress related workability can be achieved by proper die design, the intrinsic workability needs a systematic understanding of the constitutive behavior of material under given processing conditions.

The ultimate goal of any manufacturing industry is to manufacture components without macro- or microstructural defect on a repeatable basis. In recent years,

SHAILESH KUMAR SINGH, Graduate Student, and K. CHATTOPADHYAY, Professor, are with the Department of Materials Engineering, Indian Institute of Science, Bangalore 560012, India. PRADIP DUTTA, Professor, is with the Department of Mechanical Engineering, Indian Institute of Science, Bangalore 560012, India. Contact e-mail: pradip@mecheng.iisc.ernet.in

Manuscript submitted August 10, 2014.
Article published online March 28, 2015

technique of processing map based on dynamic materials model has been widely used to understand the workability of several materials in terms of the various microstructural parameters operating at different deformation conditions.^[9–17] The processing map is beneficial for optimizing hot workability and controlling the pathway of microstructure evolution in a material. With the help of a processing map, it is possible to arrive at an optimum set of parameters for designing a metal working process without resorting to expensive and time-consuming trial and error methods.

Research on semisolid processing has its origin in the early 1970s^[18–20] and has progressed substantially over the past few decades. There are literature available on mechanical and microstructure characterization of semisolid alloy below solidus temperature.^[21–26] However, to the best of our knowledge based on available literature on semisolid processing, optimization of the workability of semisolid processed components at elevated temperature in the solid state is yet to be explored. The main objectives of the present investigation is to fill this knowledge gap, study the hot workability of thixocast A356 alloy, and compare it with a conventionally cast samples of the same material. True stress data obtained from the isothermal hot compression tests in the range of temperature [573 K to 773 K (300 °C to 500 °C)] and strain rates (0.001 to 10 s⁻¹) have been used to develop the processing map. Microstructural investigation of the materials behavior is carried out in the tested samples to correlate the safe and unsafe domains with microstructural features. Moreover, analysis of the flow stress at elevated temperature is also carried out to understand and interpret the mechanism of hot deformation.

II. EXPERIMENTAL PROCEDURE

A. Material and Specimen Preparation

The material under investigation is A356 aluminum alloy, chemical composition of which is given in Table I. The material was received in the form of ingots, which were originally prepared by a conventional casting technique usually associated with formation of dendritic microstructure. These ingots were then processed with thixocasting technology consisting of two basic processes: (a) production of non-dendritic microstructure billets and (b) processing of non-dendritic billets to make components. Approximately 25 kg of A356 aluminum alloy ingot was melted in a silicon-graphite crucible in a resistance furnace set at a temperature of 1073 K (800 °C). After the alloy got completely molten, ‘cover-all’ powder (M/S Fosco) was added as a fluxing agent, facilitating the removal of oxides and guarding the melt from further oxidation. The slag formed was skimmed off. Molten aluminum alloy has tendency to vigorously dissolve hydrogen gas present in the atmosphere. As a result, aluminum alloys release excessive amount of hydrogen during solidification. This results in microporosity defects distributed throughout the solid metal. Therefore, flux in the form of hexachloroethylene

tablets weighing 50 g each (M/S Degasser 200) was plunged by a clean preheated perforated bell to the furnace bottom. The flux components react with aluminum forming gaseous compounds (aluminum chloride, aluminum fluoride) which bubble and escape through the melt. As partial pressure of hydrogen is very low, it easily diffuses from the molten aluminum into the bubbles. To compensate for the evaporation loss, magnesium (0.5 wt pct of melt weight) was added and then allowed to remain for about half an hour for getting homogenized. Additionally, Ti-B (0.1 wt pct of melt weight) and modifier of aluminum (strontium, 0.06 wt pct of melt weight) were added to the melt and allowed to soak for 10 minutes. Approximately 1.5 kg of molten metal is subsequently transferred into a crucible. When the temperature reaches 913 K (640 °C), the metal is poured into the preheated metal mold kept inside the linear electromagnetic stirrer in which shearing action produced at the solid/liquid interface results in the formation of slurry, which finally results in production of cylindrical billets with non-dendritic microstructure. The parameters chosen for the operation of electromagnetic stirrer were 300 A current at 50 Hz frequency, and stirring time was maintained for 25 seconds during each experiment. After 25 seconds of stirring action, water supply for the metal mold was switched on and immediately allowed to pass through the cooling channels to quench the metal. The billets obtained were of dimensions 230 mm in length and 75 mm in diameter. In step (b), the cylindrical billet thus obtained was sectioned to the required size before heating up to the semisolid temperature. The reheated billet was injected into a closed die of a high pressure die casting machine to get the required shaped component. Figure 1 represents a schematic of thixocasting processing route with compression and tensile specimens. Figure 2 shows the dendritic microstructure of A356 conventionally cast alloy and globular microstructure of semisolid processed A356 alloy.

Test specimens were prepared from thixocast A356 alloy bars as well as conventionally cast A356 alloy samples. Each specimen was machined in the form of cylinders with height-to-diameter ratio of 1.5. (height is 15 mm and diameter is 10 mm). During machining, it was ensured that the edges of the specimen were chamfered to avoid fold-over in the initial stages of compression. Concentric grooves of 0.5-mm depth were provided on the faces of the specimen to retain lubricant of molybdenum sulfide oil during deformation so that friction at the specimen/platens interface could be minimized. The temperature of the specimen was monitored with a thermocouple embedded in a hole of 0.8 mm diameter drilled at a location corresponding to half the height of the specimen.

B. Hot Compression Testing and Data Analysis

Compression tests were carried out at strain rates in the range of 0.001 to 10 s⁻¹ with each test done at a strain rate value one order of magnitude apart the other, and in the temperature range of 573 K to 773 K (300 °C to 500 °C) with 323 K (50 °C) interval, using a computer controlled

Table I. The Chemical Composition of Experimental Alloy (in Weight Percent)

Al	Si	Mg	Fe	Cu	Mn	Ti	Sr	Ni
Bal.	7.50	0.40	0.15	0.03	0.03	0.16	0.05	0.03

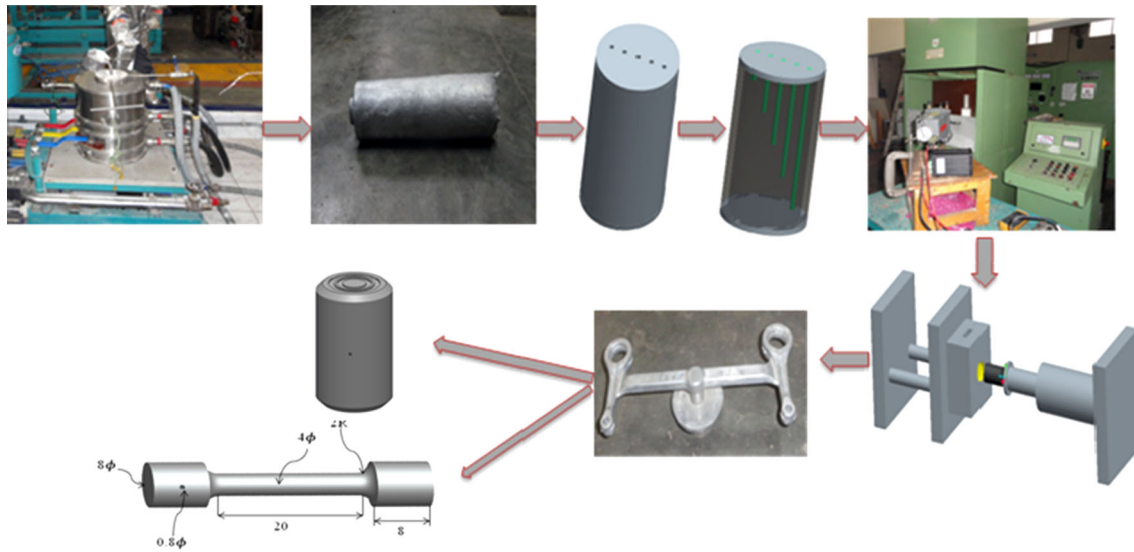


Fig. 1—Schematic of thixocast manufacturing route with compression and tensile specimen.

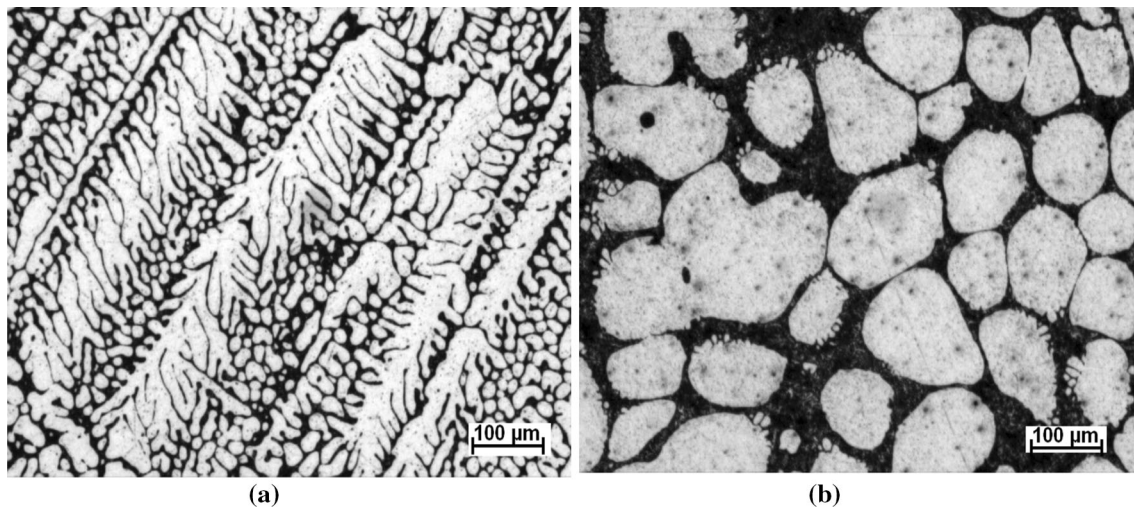


Fig. 2—(a) Initial microstructure of conventional cast A356 alloy showing dendrites typical of as-cast material and (b) Microstructure of thixocast A356 alloys showing globular α phase.

servohydraulic testing machine (DARTEC) of 100 kN capacity. A resistance heating split furnace with silicon carbide heating element was used to heat the specimen to the desired temperature by surrounding both the platens and the specimen. For each test temperature, 15 minutes of soaking time was allowed for attaining equilibrium of temperature before compressing the specimen to about half its height. The temperature was controlled within $\pm 2^\circ\text{C}$. The specimens were deformed to 50 pct, corresponding to a true strain of 0.69. The deformed samples were air cooled and then cut along the compression axis. The cut surface was mechanically polished using a

standard technique and etched electrolytically in a solution of 0.5 pct HF. The load stroke curve obtained in compression was converted to the engineering stress–strain curve and subsequently to the true stress–strain curve using standard equations. The elastic region was subtracted from the true stress–strain curve to get the true stress–true plastic strain in the range 0.05 to 0.6. The flow stress data obtained at different temperature and strain rates were corrected for the adiabatic temperature rise, if any, using linear interpolation of $\log \sigma$ vs $(1/T)$. This correction was found to be significant at lower temperatures and at high strain rates. Figure 3 shows the

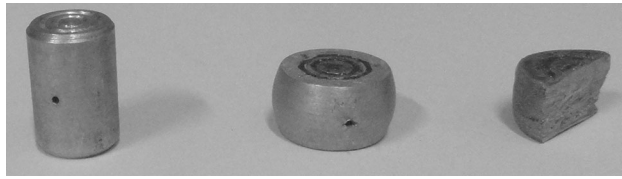


Fig. 3—Cylindrical compression specimen, deformed specimen after hot compression test and cut section for microstructure analysis.

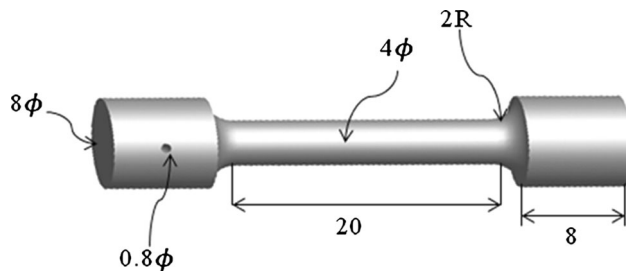


Fig. 4—Schematic diagram of tensile specimen according to ASTM E8M-01 (all dimensions are in mm).

cylindrical sample used for compression test, its deformed shape after compression and cut section for further microstructural analysis.

C. Hot Tensile Testing

To determine the ductility at elevated temperature, tensile tests were conducted for thixocast A356 aluminum alloy as well as for conventionally cast A356 alloy in the temperature range [573 K to 773 K (300 °C to 500 °C)] in an Instron screw-driven test frame of 5 kN load capacity at 0.001 s^{-1} . The tensile samples have been prepared according to ASTM E8M-01 standard with a gage length of 20 mm and gage diameter of 4 mm, as shown in Figure 4. A small hole of 0.8 mm diameter and 3-mm depth was drilled in the head portion of the sample for inserting a thermocouple which was used to monitor the temperature of the specimen during testing.

III. RESULTS AND DISCUSSION

A. Analysis of Flow Curve

The flow stress is the most basic parameter used to characterize plastic deformation properties of metals and alloys, and the flow stress of metals determines the size of load and energy needed during plastic deformation. The nature of the stress-strain curves provides information related to the mechanisms of hot deformation.^[27]

The flow curves obtained for thixocast A356 and conventionally cast A356 at a strain rate of 1 s^{-1} and temperature range [573 K to 773 K (300 °C to 500 °C)] are presented in Figure 5. The flow stress as well as the shape of the flow curves are dependent of temperature and strain rate. A comparison of the curves reveals that, for a specific strain rate, the flow stress decreases remarkably with increasing temperature. In contrast,

for a fixed temperature, the flow stress generally increases with strain rate due to an increase in dislocation density and the rate of dislocation multiplication. It is also observed that stress level decreases with increasing deformation temperature and decreasing strain rate. This is because lower strain rate and higher temperature provide longer time for energy accumulation and higher mobilities at boundaries for nucleation and generation of dynamic recrystallized grains and dislocation annihilation, and thus reduce the flow stress level.

It is observed from Figure 5(a) that for the range of deformation temperature used in the present investigation [*i.e.*, 573 K to 773 K (300 °C to 500 °C)], flow stress curves of thixocast A356 alloy exhibit a single and smooth peak at critical strain followed by a nearly steady behavior. It is reasonable to presume that the softening mechanism under these conditions may be due to dynamic recrystallization (DRX). However, for conventionally cast A356 alloy sample (Figure 5(b)), such a prominent peak is not noticed. The degree of dynamic softening beyond true strain of 0.1 is considerably smaller during deformation at the higher temperature of 673 K, 723 K and 773 K (400 °C, 450 °C and 500 °C) for thixocast A356 alloy, as seen from Figure 5(a). At these temperatures, a nearly horizontal curve is obtained, indicating a steady state, independent of further strain. This suggests that the rate of thermal softening at this stage is balanced by the rate of work hardening. This behavior of the flow curve is an indication of dynamic recovery (DRV).

On comparing the flow stresses at elevated temperatures [in the range 573 K to 773 K (300 °C to 500 °C)] of thixocast and conventionally cast A356 alloy samples, the latter showed higher value at different strain levels, temperatures, and strain rates. This indicates that the flow property of thixocast alloy is better than the conventionally cast material as it requires lower energy for the material to flow at elevated temperature (*i.e.*, response to plastic flow is better for thixocast alloy).

In order to quantify the effect of temperature on strain hardening, the slope of stress strain curve (*i.e.*, $\theta = \frac{\partial \sigma}{\partial \epsilon}$) is plotted against temperature. The plot of θ vs T for thixocast A356 alloy at strain rate 1 s^{-1} for strain of 0.1 and 0.5 is given in Figure 6(a). The figure indicates that the thixocast A356 alloys for a strain of 0.1 shows increase in flow softening with temperature, with maximum softening effect observed at 773 K (500 °C). Such a decrease in flow stress is due to occurrence of DRX, as higher temperature offers higher mobility to grain boundaries. Again, for a strain level of 0.5, there is slight flow softening in the temperature range 573 K to 673 K (300 °C to 400 °C). However, in the temperature range 673 K to 773 K (400 °C to 500 °C), a nearly horizontal line is obtained which suggests that the rate of thermal softening is balanced by the rate of work hardening. It could be observed that the effect of temperature on strain hardening is more significant at lower strain levels. Similarly, a plot of θ vs T for conventionally cast A356 alloy at strain rate 1 s^{-1} for strains of 0.1 and 0.5 is shown in Figure 6(b). This plot indicates that in the temperature range 573 K to 623 K

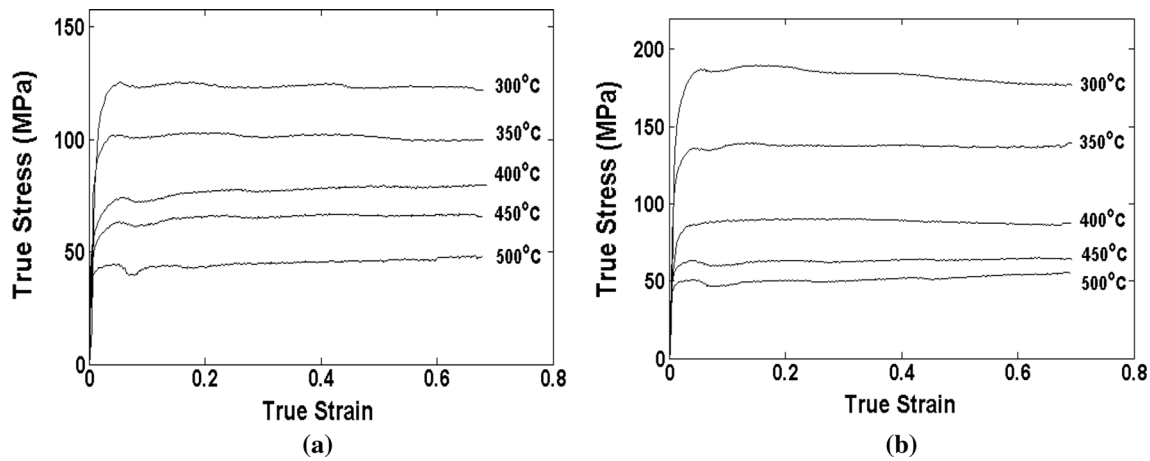


Fig. 5—True stress–True strain curves of (a) Thixcast A356 aluminum alloy and (b) conventionally cast A356 aluminum alloy during hot compression deformation at $\dot{\epsilon} = 1 \text{ s}^{-1}$.

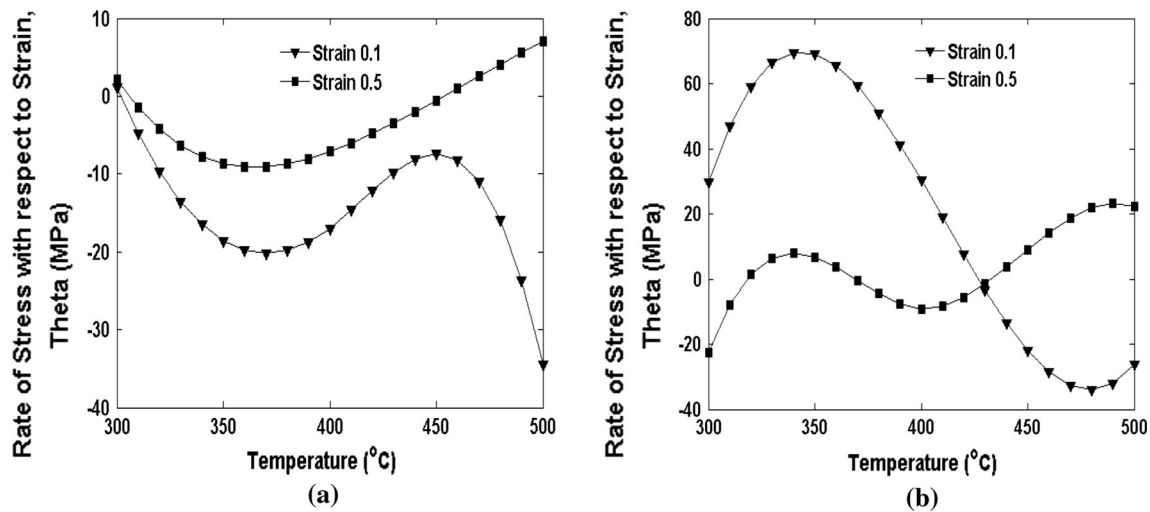


Fig. 6—Plot of Theta vs Temp for (a) thixcast A356 aluminum alloy and (b) conventionally cast A356 aluminum alloy at strain rate 1 s^{-1} .

(300 °C to 350 °C), there is a marginal strain hardening. This is followed by the increase in flow softening in the temperature range 673 K to 773 K (400 °C to 500 °C), while at strain level 0.5 there is flow softening noticed at the temperature range of 573 K to 673 K (300 °C to 400 °C). However, with further rise in temperature the change in softening effect is negligible. It could be observed that the effect of temperature on strain hardening is more significant at lower strain levels for both thixcast as well as conventionally cast A356 alloy.

It is also important to study the effect of temperature on strain rate when the flow behavior is studied over a wider domain of strain rate and temperature. In order to study the relationship of strain rate hardening with temperature and strain, the strain rate sensitivity ($m = \frac{\partial \ln \sigma}{\partial \ln \dot{\epsilon}}$) was plotted against temperature. The plot of m vs T for thixcast A356 alloy at strain levels 0.1 and 0.5 is shown in Figure 7(a). It indicates that for thixcast A356 alloy, the strain rate sensitivity (m) increases with temperature for both the strain levels. A similar behavior is also observed in conventionally cast

A356 alloy, as shown in Figure 7(b). Thus, from the behavior of strain rate sensitivity to temperature at different strain levels, it can be concluded that the strain rate sensitivity is almost independent of strain for both alloy samples.

B. Ductility Test

Similarly, ductility is an important parameter for determining the plasticity of a material. It is not only important for preventing fracture, but it also reduces the effect of stress concentration. Figure 8 compares the yield stress and elongation to failure of thixcast A356 sample and conventionally cast sample of the same alloy. It is found that the thixcast sample yields at a lower value in comparison to conventionally cast sample at elevated temperature. However, elongation to failure of thixcast alloy is higher than that of the latter. This further confirms that the workability of thixcast components is better than conventionally cast parts at elevated temperature. This property makes it more

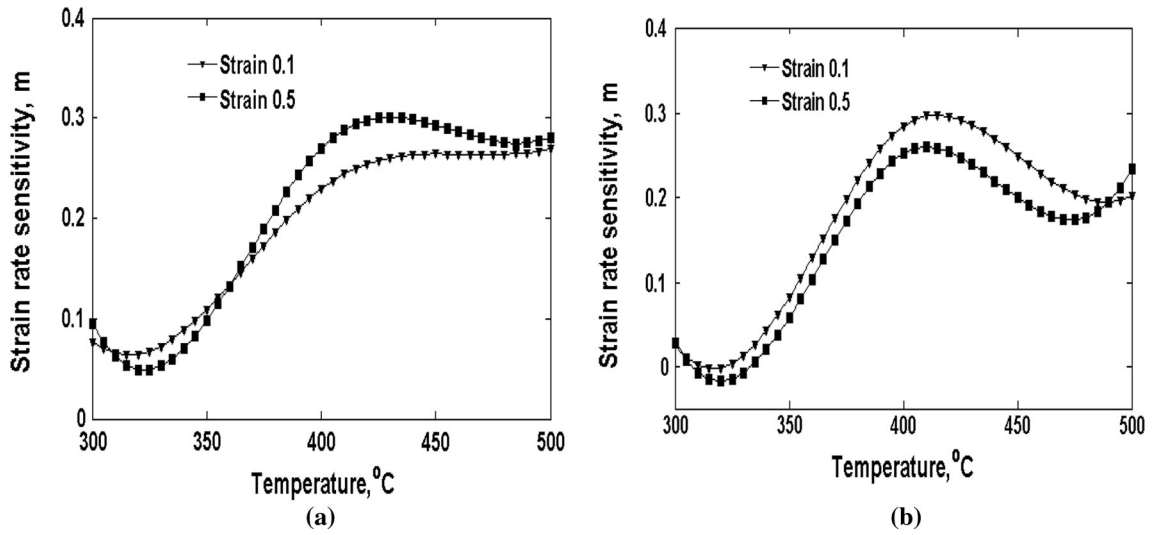


Fig. 7—Plot of m vs Temp for (a) Thixocast A356 aluminum alloy and (b) conventionally cast A356 aluminum alloy at strain rate 1 s^{-1} .

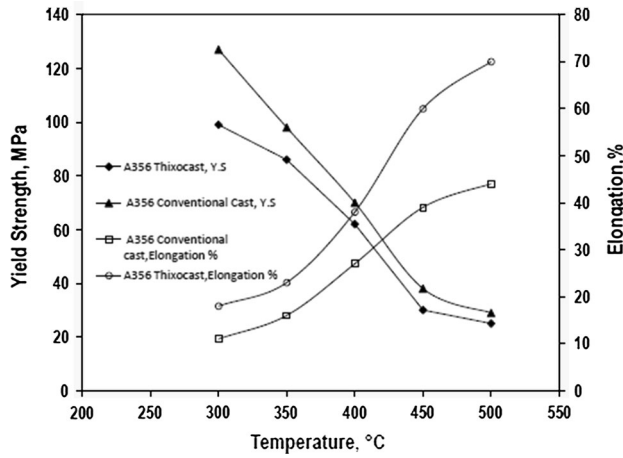


Fig. 8—Variation of yield strength and percentage elongation with temperature for thixocast and conventionally cast A356 aluminum alloy.

suitable for thixo-forming at an elevated temperature. At the same time, the thixocast components have better yield strength at room temperature than those of conventional cast parts. Thixocast A356 alloy at room temperature exhibits yield strength of 135 MPa, while conventionally cast A356 alloy of same material shows 111 MPa.

C. Processing Map and Its Interpretation

In order to identify the region which is suitable and safe for carrying out a thermomechanical process, a processing map based on the dynamic material model^[27,28] is developed. It is obtained by superimposition of the instability maps over the power dissipation maps. Power dissipation maps depict, in a frame of temperature and strain rates, the pattern in which material dissipates the power through the microstructural changes. According to DMM, the work piece subjected

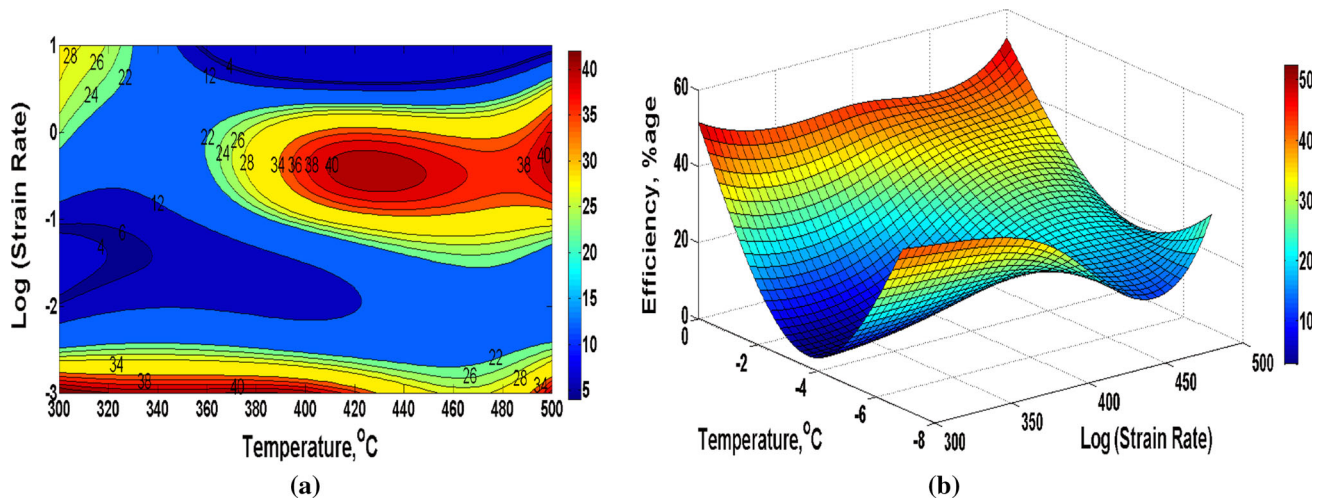


Fig. 9—Power dissipation map in (a) 2D and (b) 3D, respectively, for thixocast A356 aluminum alloy.

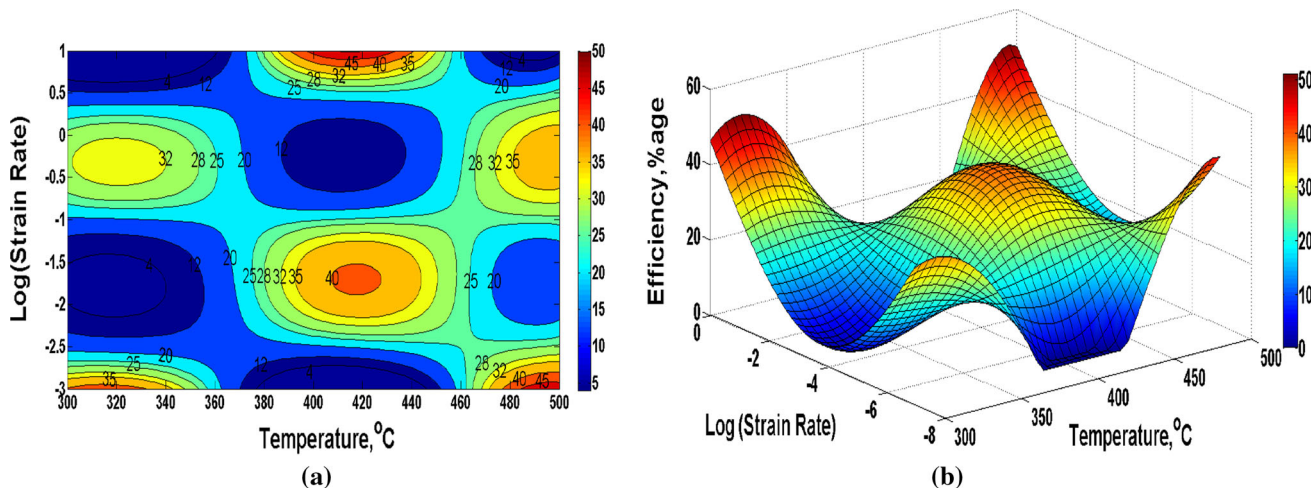


Fig. 10—Power dissipation map in (a) 2D and (b) 3D, respectively, for conventionally cast A356 aluminum alloy.

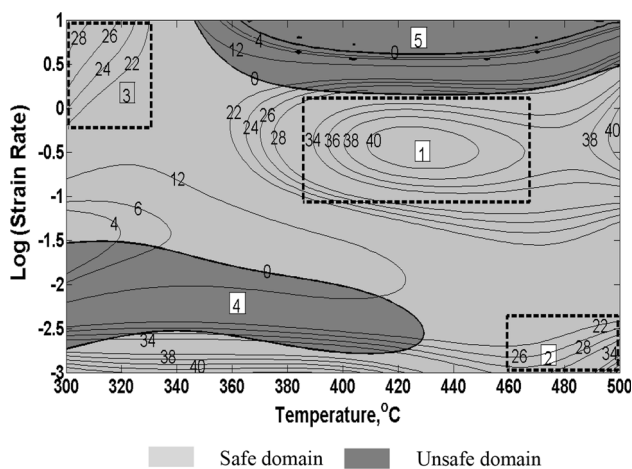


Fig. 11—Processing map for thixocast A356 Aluminum alloy at a true strain of 0.5.

to hot deformation is assumed to be a non-linear dissipator of power and hence does not store significant amount of energy. Efficiency Parameter is therefore used to specify the power dissipated through various mechanisms involved during deformation of material. The variation of efficiency parameter is plotted in temperatures and strain rates frame to develop a map called ‘power dissipation map’ or ‘efficiency map.’

The processing map exhibits various safe and unsafe domains which are the characteristics of deformation mechanism involved during the hot working. The safe domain represents the suitability of the materials to exhibit thermomechanical processing. It identifies the region for processing the material with desirable microstructure and superior mechanical properties. It helps in designing the thermomechanical processes by optimizing the process variables like temperature and strain rate to achieve a defect-free component with desired microstructure. Unsafe domain represents the regimes of temperature and strain rate where deformation is not homogeneous and creates microstructural

defects. The inhomogeneous deformation is not desirable for the product performance, particularly with respect to ductility and fracture toughness. Figure 9 shows the power dissipation map for thixocast A356 alloy. The contours represent constant efficiency of power dissipation for various percentage values of dissipation. It is observed from Figure 9(a) that there is wide variation of efficiency with a maximum of 40 pct to a minimum of 4 pct. The lower efficiency indicates the negligible effect of strain rate sensitivity which ultimately has an impact on poor ductility, while higher efficiency indicates the safe working region with the mechanism of DRX and DRV is being the predominant ones. Generally, the efficiency values associated with such mechanisms are about 35 to 45 pct for DRX^[27,29–31] and 20 to 30 pct for DRV.^[27] The lower efficiency values for DRV are due to the less effective energy dissipation through dislocation annihilation compared to DRX, in which the migration of interfaces also contribute to annihilation of a large number of dislocations. The higher efficiency region in the map is shown by reddish color, while the lower efficiency region is demarcated by dark bluish color. The power dissipation map can also be plotted in 3D as shown in Figure 9(b), depicting the increase (hills) or decrease (valleys) of the power dissipation parameter. A hill represents efficiency domains, and each domain in the map represents a specific microstructural mechanism that contributes to the power dissipation. A valley corresponds to a bifurcation separating the domains. Similarly, Figures 10(a), (b) shows the power dissipation map in 2D and 3D, respectively, for conventionally cast A356 aluminum alloy. Here, efficiency variation is from 45 to 4 pct. Even if the efficiency is high in a region, there is likelihood that the region may not be suitable for thermomechanical processing because of the flow localization and adiabatic shear band formation. Hence, it becomes extremely important to include the instability criteria in power dissipation maps to obtain processing maps providing useful information about the workability of the materials. On the basis of the above discussion, the different domains obtained in the pro-

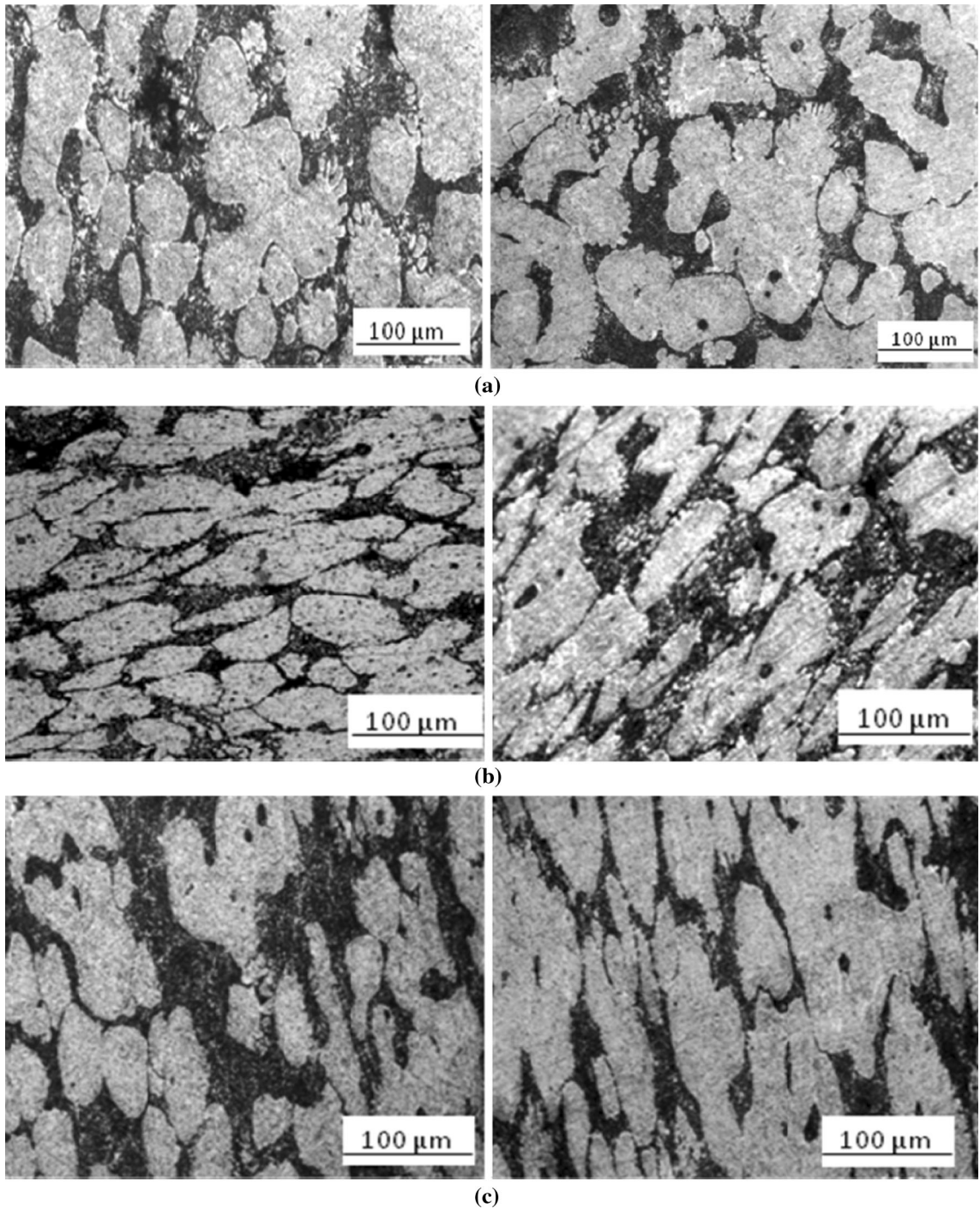


Fig. 12—Typical microstructure of the thixcast A356 alloy specimen in safe domain (a) domain 1 (b) domain 2 and (c) domain 3.

cessing maps of thixcast and conventionally cast A356 samples are discussed subsequently.

D. Processing Map of Thixcast A356 Aluminum Alloy

The processing map of thixcast A356 alloy, as shown in Figure 11, exhibits three domains in a stable region and two domains that represent the unstable regions. Domain 1 lies in the stable region with the peak efficiency of 40 pct, which has occurred at a temperature

of 703 K (430 °C) and strain rate of 0.5 s^{-1} . The nature of the efficiency hill indicates that the domain is not a steep one. The efficiency variation is from 34 to 40 pct and it is spread over wide ranges of temperature [663 K to 738 K (390 °C to 465 °C)] and strain rate (0.1 to 1 s^{-1}). The high efficiency of power dissipation indicates that DRX is the key mechanism involved in the deformation at this domain. The microstructures of the specimens deformed in this domain characterized by a strain rate range of 0.1 to 1.0 s^{-1} and temperature

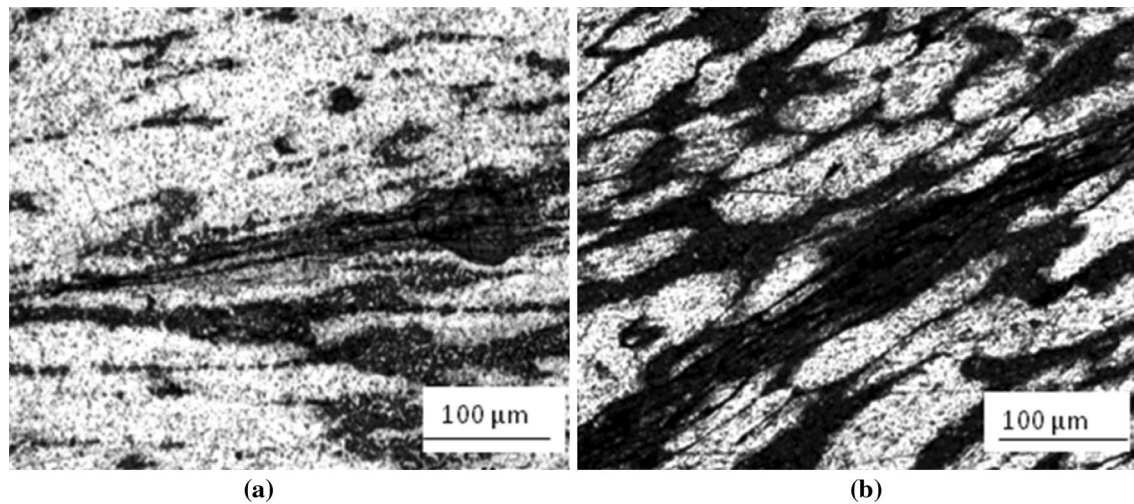


Fig. 13—Typical microstructure of the thixcast A356 alloy specimen in unsafe domain (a) domain 4 and (b) domain 5.

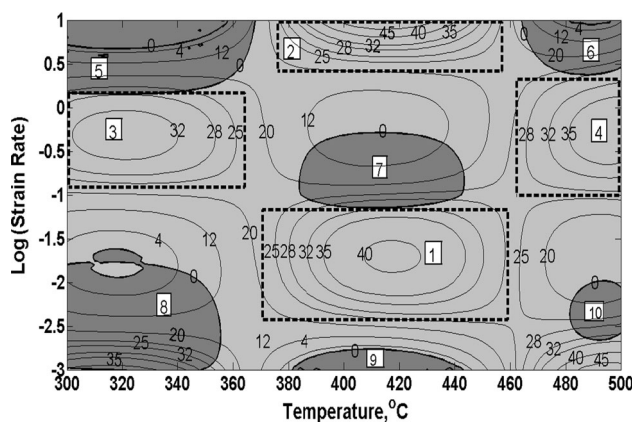


Fig. 14—Processing map of conventionally cast A356 Aluminum alloy at a true strain of 0.5.

range between 673 K and 723 K (400 °C and 450 °C) are shown in Figure 12(a). The microstructures reveal the presence of defect-free equiaxed α phase grains as well as the nucleation and growth of newer α phase grains. This feature represents the DRX mechanism. Domain 2 is a narrow one for safe processing with a peak efficiency of 34 pct, which has occurred at 773 K (500 °C) and at a strain rate of 0.001 s^{-1} . The efficiency variation is from 28 to 34 pct and this spreads over a temperature range [733 K to 773 K (460 °C to 500 °C)] and strain rate range (0.001 to 0.01 s^{-1}). The representative microstructure of the specimen tested in this domain is shown in Figure 12(b) which reveals that the substructures in the deformed specimens consist of very small amounts of fine precipitates with equiaxed polygonized sub-grains in the elongated grains, providing the evidence for DRX. Domain 3 is another safe domain for processing with a peak efficiency of 28 pct, which has occurred at a temperature and strain rate of 573 K (300 °C) and 10 s^{-1} , respectively. The representative microstructure of the specimen tested in this domain has been shown in Figure 12(c). It appears to be dynamical-

ly recovered, and repolygonization of microstructure was observed.

The instability regions on the processing map are demarcated from the stable flow region as shown in Figure 11. Domain 5 occurs at high strain rates (*i.e.*, 10 to 2 s^{-1}) and in the temperature range of 623 K to 773 K (350 °C to 500 °C). The representative microstructure of the specimen tested in this domain is shown in Figure 13(a). The microstructure reveals manifestation of instability in the form of adiabatic shear bands which are oriented at 45 degrees to the compression axis. At higher strain rates, heat generated due to plastic deformation is not able to diffuse toward the cooler parts of the specimen in a short time. Hence, the flow stress decreases and further plastic flow get localized. The bands become intensified and nearly satisfy adiabatic conditions.^[32,33] Hence, these are called adiabatic shear bands. Domain 4 occurs at low strain rate range (0.002 to 0.2 s^{-1}) and temperature [*i.e.*, 573 K to 703 K (300 °C to 430 °C)]. The microstructure corresponding to the specimen deformed in this regime is shown in Figure 13(b), which indicates inhomogeneous deformation.

E. Processing Map of Conventionally Cast A356 Aluminum Alloy

The processing map of conventionally cast A356 alloy obtained at strain rate $\dot{\epsilon} = 0.5$ is shown in Figure 14. There are four distinct domains (1 to 4) in the stable region and four more domains (5 to 8) represent the unstable region. Domain 1 is a safe domain of processing with a peak efficiency of 35 pct occurring at 693 K (420 °C) and 0.03 s^{-1} . The efficiency variation is from 25 to 35 pct in the temperature range from 653 K to 733 K (380 °C to 460 °C) and strain rate range (0.005 to 0.1 s^{-1}). Microstructure of the specimen corresponding to this domain is shown in the Figure 15(a). Domain 2 with a peak efficiency of 45 pct occurred at 410 °C/ 10 s^{-1} . The nature of the efficiency hill suggests that the domain is steep. The efficiency variation occurs from 25

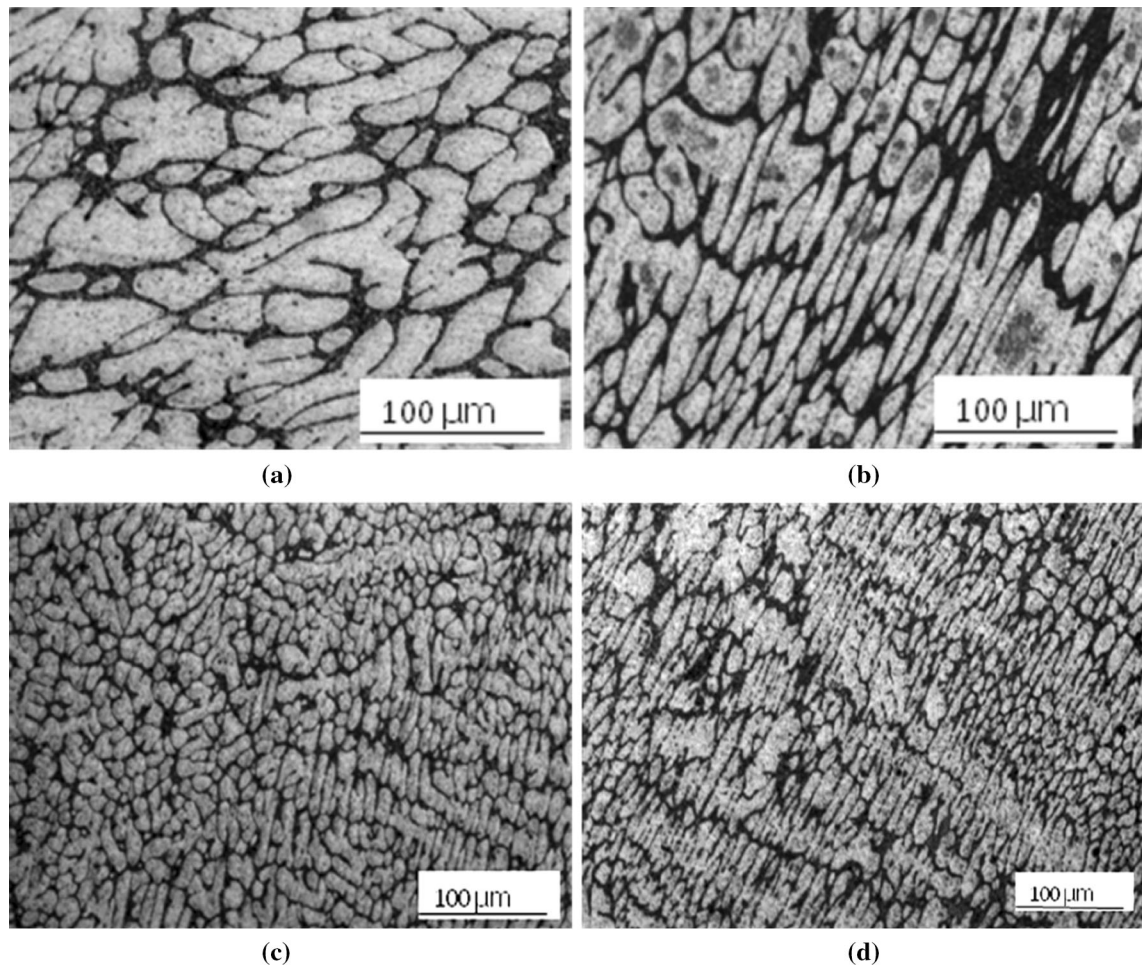


Fig. 15—Typical microstructure of the conventionally cast A356 aluminum alloy specimen in safe domain (a) domain 1, (b) domain 2, (c) domain 3 and (d) domain 4.

to 45 pct and is in the temperature range [643 K to 733 K (370 °C to 460 °C)] and strain rate range (4 to 10 s^{-1}). The contours involving DRX and DRV domains are generally wide spread, indicating a steep hill. The representative microstructure of the specimen in this domain is given in Figure 15(b). On comparison with the initial microstructure, a large extent of reconstitution in the primary phase morphology is observed. The as-cast dendritic structure is completely broken; globularization of α phase has occurred and certain waviness in α phase boundaries is noticed. A similar feature was also observed in the case of α - β brass.^[34] This confirms that the α phase has undergone DRV. Similarly, domain 3 with a peak efficiency of 35 pct at 593 K (320 °C) and 0.5 s^{-1} is spread over 573 K to 623 K (300 °C to 350 °C) and 0.1 to 1.0 s^{-1} , while domain 4 with peak efficiency of 35 pct is spread over 733 K to 773 K (460 °C to 500 °C) and 0.1 to 1.0 s^{-1} . These domains indicate that dynamic recovery is the main softening mechanism. Microstructure of the specimen corresponding to this domain is shown in Figures 15(c), (d).

The six instability regions on the processing map are demarcated from the stable region as shown in Figure 11. The instability domains 5 and 6 occur at high strain rates

(1 to 10 s^{-1}), domain 7 occurs at an intermediate strain rate (0.2 to 0.6 s^{-1}), while domain 8, 9, and 10 occur at low strain rates (10^{-3} to 10^{-2} s^{-1}). Domain 5 occurs in the temperature range [573 K to 623 K (300 °C to 350 °C)] and domain 6 lies in the temperature range [733 K to 773 K (460 °C to 500 °C)]. Microstructure corresponding to this domain is shown in Figures 16(a), (b) which shows that the instability is manifested in the form of adiabatic shear band. Domain 7 is a narrow unsafe domain which falls in the intermediate strain rate and temperature ranges [*i.e.*, 653 K to 713 K (380 °C to 440 °C)]. Microstructure of the specimen corresponding to this domain is shown in Figure 16(c) which indicates inhomogeneous deformation. Similarly, domain 8 occurs in the temperature range [573 K to 623 K (300 °C to 350 °C)]. This domain exhibits an efficiency peak of 35 pct. However, the instability parameter becomes negative here and the domain falls under unsafe category. The microstructure of the specimen deformed in this region is shown in Figure 16(d). The microstructure shows localization; discontinuous deformation often localizes in narrow zones and the neighboring regions remain intact. Similarly, domain 9 and 10 are narrow ones in the low strain rate regime. Domain 9 occurs in the temperature range [*i.e.*, 653 K to 713 K (380 °C to

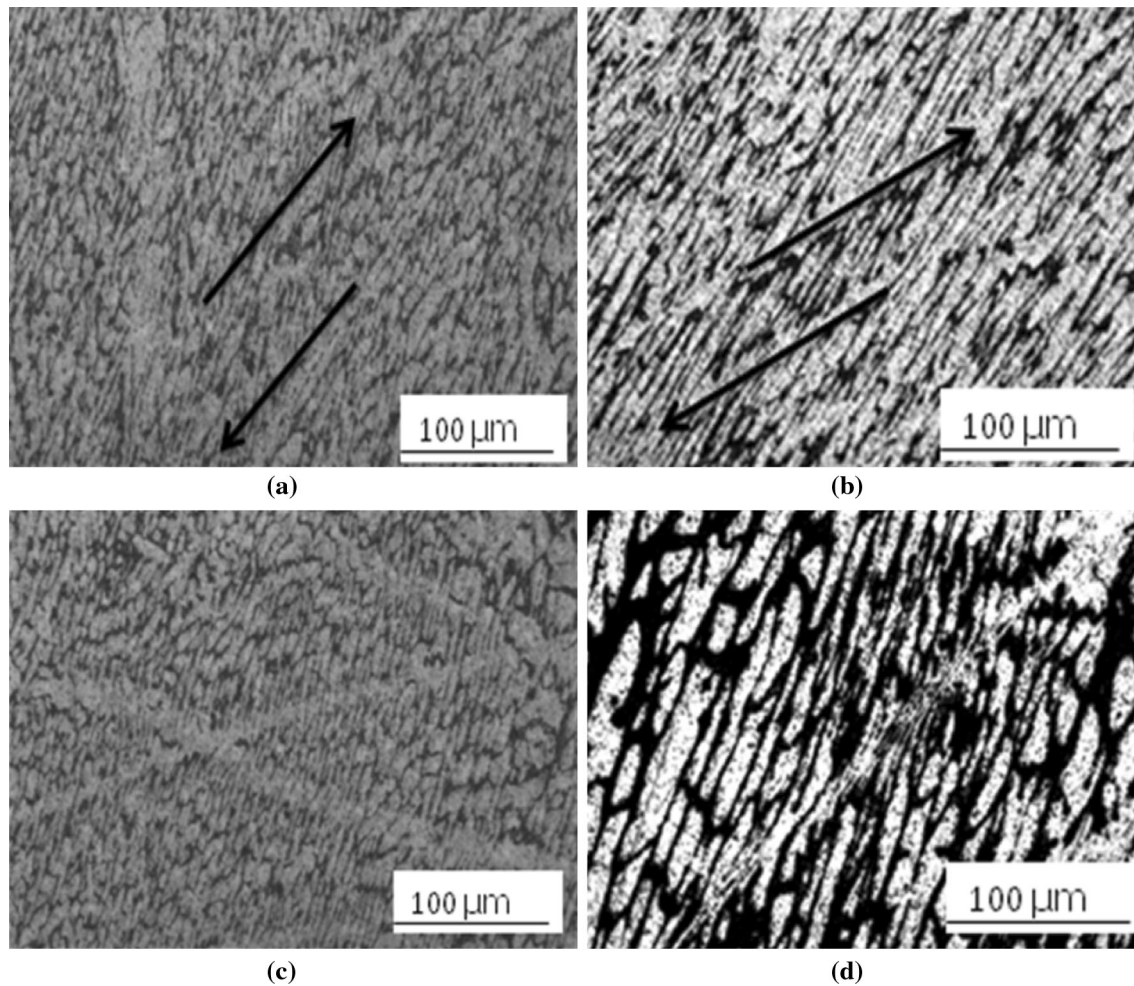


Fig. 16—Typical microstructure of the conventionally cast A356 aluminum alloy specimen in unsafe domain (a) domain 5, (b) domain 6, (c) domain 7 and (d) domain 8.

440 °C)] and domain 10 in the temperature range [*i.e.*, 753 K to 773 K (480 °C to 500 °C)].

IV. CONCLUSIONS

A comparative study of high-temperature workability of thixocast and conventionally cast A356 Aluminum alloy was carried out. The study highlights the response to plastic flow by changing the microstructure to globular form. Thixocast alloy exhibits better flow property at elevated temperature as compared to the conventionally cast alloy. The strain rate sensitivity of the investigated alloy is found to be independent of the strain level. In addition, the processing map helps in identifying the safe regions (*i.e.*, strain rate and temperature) for carrying out the thermomechanical processing of semisolid processed A356 aluminum alloy. In summary, this study describes the flow behavior of thixocast and conventionally cast alloy at various temperature and strain rates, which provides useful information for selecting appropriate constitutive equations.

REFERENCES

1. K. Siriporn, S. Wisutmethangoon, T. Plookpholi, and J. Wannasin: *JOM*, 2008, vol. 18, pp. 93–97.
2. M.C. Flemings and R. Mehrabian: *AFS Trans.*, 1973, vol. 102, pp. 81–88.
3. T. Matsumiya and M.C. Flemings: *Metall. Trans. B*, 1981, vol. 21, pp. 17–31.
4. P. Kapranos, P.J. Ward, H.V. Atkinson, and D.H. Kirkwood: *Mater. Des.*, 2000, vol. 21 (4), pp. 387–94.
5. Z. Fan: *Int. Mater. Rev.*, 2002, vol. 47 (2), pp. 49–85.
6. D. Brabazon, D.J. Browne, and A.J. Carr: *Mater. Sci. Eng. A*, 2003, vol. 356, pp. 69–80.
7. S.N. Aqida, M. Maurel, D. Brabazon, S. Naher, and M. Rosso: *Int. J. Mater. Form.*, 2009, vol. 2, pp. 761–64.
8. S.K. Singh, K. Chattopadhyay, G. Phanikumar, and P. Dutta: *Acta Mater.*, 2014, vol. 73, pp. 177–85.
9. S. Venugopal, S.L. Mannan, and Y.V.R.K. Prasad: *Mater. Lett.*, 1992, vol. 15, pp. 79–83.
10. S. Venugopal, S.L. Mannan, and Y.V.R.K. Prasad: *Mater. Sci. Eng. A*, 1994, vol. 177, pp. 143–49.
11. P.V. Sivaprasad, S.L. Mannan, and Y.V.R.K. Prasad: *Mater. Sci. Technol.*, 2004, vol. 20, pp. 1545–50.
12. B. Paul, R. Kapoor, J.K. Chakravarty, A.C. Bidaye, I.G. Sharma, and A.K. Suri: *Scripta Mater.*, 2009, vol. 60, pp. 104–07.
13. Y.V.R.K. Prasad and K.P. Rao: *Mater. Sci. Eng. A*, 2008, vol. 487, pp. 316–27.
14. K.P. Rao, Y.V.R.K. Prasad, N. Hort, and K.U. Kainer: *J. Mater. Process. Technol.*, 2008, vol. 201, pp. 359–63.

15. Y.V.R.K. Prasad and K.P. Rao: *Mater. Sci. Eng. A*, 2008, vol. 487, pp. 316–27.
16. Y. Niu, H. Hou, M. Li, and Z. Li: *Mater. Sci. Eng. A*, 2008, vol. 492, pp. 24–28.
17. H.Z. Li, H.J. Wang, X.P. Liang, H.T. Liu, Y. Liu, and X.M. Zhang: *Mater. Sci. Eng. A*, 2011, vol. 528, pp. 1548–52.
18. D.B. Spencer: PhD. Thesis, MIT, 1971.
19. D.B. Spencer, R. Mehrabian, and M.C. Flemings: *Metall. Trans.*, 1972, vol. 3, pp. 1925–32.
20. M.C. Flemings, R.G. Riek, and K.P. Young: *Mater. Sci. Eng.*, 1976, vol. 25, pp. 103–17.
21. J. Cheng, D. Apelian, and R.D. Doherty: *Metall. Trans. A*, 1986, vol. 17A, pp. 2049–62.
22. W.G. Cho and C.G. Kang: *J. Mater. Process. Technol.*, 2000, vol. 105, pp. 269–77.
23. E.J. Zoqui, M. Paes, and E. Es-Sadiqi: *J. Mater. Process. Technol.*, 2002, vol. 120, pp. 365–73.
24. H.V. Atkinson: *Prog. Mater. Sci.*, 2005, vol. 50, pp. 341–412.
25. G. Hirt and R. Kopp: *Thixoforming, Semi-Solid Metal Processing*, Wiley, New York, 2009.
26. M. Theron, R.D. Knutsen, L.H. Ivanchev, and H.P. Burger: *J. Mater. Process. Technol.*, 2012, vol. 212, pp. 465–70.
27. Y.V.R.K. Prasad and S. Sasidhara: *A Compendium of Processing Maps*, ASM International, Metals Park, 1997.
28. Y.V.R.K. Prasad, H.L. Giegel, S.M. Doraivelu, J.C. Malas, J.T. Morgan, K.A. Lark, and D.R. Barker: *Metall. Trans. A*, 1984, vol. 15, pp. 1883–92.
29. N. Ravichandran and Y.V.R.K. Prasad: *Metall. Trans. A*, 1991, vol. 22A, pp. 2339–48.
30. N. Srinivasan and Y.V.R.K. Prasad: *Mater. Sci. Technol.*, 1992, vol. 8, pp. 206–12.
31. O. Sivakesavam, I.S. Rao, and Y.V.R.K. Prasad: *Mater. Sci. Technol.*, 1993, vol. 9, pp. 805–10.
32. S.V. Narayanamurthy, B. Nageswararao, and B.P. Kashyap: *Int. Mater. Rev.*, 2000, vol. 45, pp. 15–21.
33. Y.V.R.K. Prasad, T. Seshacharyalu, S.C. Medeiros, and W.G. Frazier: *Mater. Sci. Technol.*, 2000, vol. 16, pp. 511–16.
34. D. Padmavardhani and Y.V.R.K. Prasad: *Metall. Trans. A*, 1991, vol. 22A, pp. 2985–92.